Measurements and Modeling of HO_2 Formation in the Reactions of *n*-C_3H_7 and *i*-C_3H_7 Radicals with O_2[†]

Edgar G. Estupiñán, Stephen J. Klippenstein, and Craig A. Taatjes*

Combustion Research Facility, Mail Stop 9055, Sandia National Laboratories, Livermore, California 94551-0969

Received: August 3, 2004; In Final Form: November 6, 2004

The formation of HO_2 in the reactions of C_2H_5, *n*-C_3H_7, and *i*-C_3H_7 radicals with O_2 is investigated using the technique of laser photolysis/long-path frequency-modulation spectroscopy. The alkyl radicals are formed by 266 nm photolysis of alkyl iodides. The formation of HO_2 from the subsequent reaction of the alkyl radicals with O_2 is followed by infrared frequency-modulation spectroscopy. The concentration of I atoms is simultaneously monitored by direct absorption of a second laser probe on the spin−orbit transition. The measured profiles are compared to a kinetic model taken from time-resolved master-equation results based on previously published ab initio characterizations of the relevant stationary points on the potential-energy surface. The ab initio energies are adjusted to produce agreement with the present experimental data and with available literature studies. The isomer specificity of the present results enables refinement of the model for *i*-$C_3H_7 + O_2$ and improved agreement with experimental measurements of HO_2 production in propane oxidation.

Introduction

The reaction between alkyl radicals, R, and molecular oxygen plays a pivotal role in the oxidation mechanism of alkanes at low temperatures. Complete understanding of the $R + O_2$ mechanism has implications in diverse areas such as combustion chemistry (including autoignition and engine knock), atmospheric chemistry, and radical reaction chemistry. The properties of these reactions cause a change in the mechanism of alkane oxidation between approximately 500 and 800 K, which results in the "negative temperature coefficient" behavior in hydrocarbon oxidation. The precise mechanism of the $R + O_2$ reactions has attracted much interest and has been a source of confusion and controversy. Nevertheless, a fairly detailed model of the mechanism has recently emerged thanks to the large number of experimental and theoretical studies that have been conducted. The initial step in $R + O_2$ reactions involves the formation of an alkylperoxy complex, RO_2, that can subsequently dissociate or isomerize:

$$R + O_2 \leftrightarrow RO_2 \tag{1a}$$

Direct elimination of HO_2 from the RO_2 radical is the principal mechanism for alkene + HO_2 formation:[1−6]

$$RO_2 \rightarrow \text{alkene} + HO_2 \tag{1b}$$

Alternatively, the RO_2 radical can isomerize via intramolecular hydrogen transfer to form a variety of different hydroperoxyalkyl radicals, usually denoted as QOOH:

$$RO_2 \rightarrow QOOH \tag{1c}$$

Decomposition of the QOOH species via O−O bond fission provides the primary route of OH formation:

$$QOOH \rightarrow \text{O−heterocycle} + OH \tag{1d}$$

Branching between OH and HO_2 via reactions 1d and 1d is important for chain propagation because of the different reactivities of the two radicals. In addition, the reactions of QOOH with O_2 are thought to be responsible for chain branching at low temperatures (∼600−800 K).[7,8] The complexity of possible isomerization pathways in higher-hydrocarbon-radical reactions leads naturally to an effort to build general models on the basis of simpler, more easily characterized systems. The ethyl (C_2H_5) + O_2 system is the most extensively studied of the alkyl + O_2 reactions both experimentally[2,6,9−20] and theoretically.[1,3,5,19−27] The reaction of the ethyl radical with O_2 is considered the "prototype" alkyl + O_2 reaction because it is the smallest system where alkene formation and isomerization to QOOH are possible.

Recently, the time-dependent production of HO_2 and OH has been measured for several photolytically initiated alkane oxidation systems.[2,20,28−31] The experimental results have been compared to detailed master-equation calculations based on ab initio characterizations of the potential-energy surfaces for the reactions combined with integrated rate equation models that include both radical formation and radical destruction reactions that occur among species present in the experiment.[3,5,20,31] The models accurately describe the time behavior and amplitude of HO_2 from Cl-initiated oxidation of both C_2H_6 and C_3H_8.[20,31] However, the models underpredict the amount of OH observed at high temperatures (>600 K) and overpredict the amount of OH observed at lower temperatures (although uncertainties in the rate coefficients of some key reactions involving OH affect the model results).[20] The results of these comparisons emphasize several important aspects of $R + O_2$ systems. First, it is essential to include formally direct pathways for chemically activated reactions. In other words, one must include reactions from the reactants to each of the unimolecular and bimolecular products, from each of the unimolecular species to every other one, and from each of the unimolecular species to the bimolecular products. For example, direct HO_2 production from $R + O_2$ must be included. This reaction does not represent a separate abstraction mechanism but an immediate production of HO_2 via

[†] Part of the special issue "George W. Flynn Festschrift".

* Corresponding author. E-mail: cataatj@sandia.gov.

10.1021/jp046514s CCC: $30.25
Published on Web 02/09/2005

rapid dissociation of a chemically activated RO_2* prior to collisional stabilization. The master-equation results also emphasize the rapid reversibility of the $RO_2 \leftrightarrow$ QOOH isomerizations under most experimental conditions. Finally, experimental and theoretical studies on the butyl + O_2[31] and neopentyl + O_2[29] systems have suggested that master-equation solutions for a smaller system can be extended to effectively model analogous, larger R + O_2 systems.

In the present work, time-resolved production of HO_2 from the reactions of ethyl, *n*-propyl, and *i*-propyl radicals with O_2 is measured as a function of temperature and pressure in the "transition region" between 623 and 703 K. The present investigation uses photolysis of alkyl iodides to initiate the reactions and extends the scope of earlier work in one very important aspect: direct photolysis studies allow independent determinations of HO_2 production in the reactions of the two propyl isomers (*n*-propyl and *i*-propyl) with O_2 in the "transition region". Experimental measurements, both pulsed-photolytic Cl-initiated oxidation experiments conducted previously[20,28,31] and the present results using direct photolysis of ethyl, *n*-propyl, and *i*-propyl iodides, are compared to kinetic models based on the results of time-dependent master-equation calculations with ab initio characterization of stationary points. In the course of these experiments, the branching fraction of spin−orbit-excited iodine atoms, I($^2P_{1/2}$) (denoted I*), following the photodissociation of ethyl, *n*-propyl, and *i*-propyl iodides at 266 nm is measured by using time-resolved laser gain versus absorption spectroscopy.

Methods

Experiment. The reactions of ethyl (C_2H_5) and propyl (C_3H_7) radicals with O_2 are investigated using a modification of the laser photolysis−continuous-wave infrared two-tone frequency-modulation (FM) method employed previously for other R + O_2 reactions.[2,20,28−32] Ethyl, *n*-propyl, and *i*-propyl radicals are generated by 266 nm photolysis of ethyl, 1-propyl, and 2-propyl iodides:

$$RI + h\nu\ (266\ nm) \rightarrow I(^2P_{1/2},^2P_{3/2}) + R \qquad (2)$$

The HO_2 radical is monitored by laser probing in the 000-000 band of the $\tilde{A}^2A' \rightarrow \tilde{X}^2A''$ electronic transition near 1.4 μm.[33] The concentration of I atoms is deduced from a simultaneous measurement of the absorption on the spin−orbit transition of the I-atom photolysis coproduct, permitting transient HO_2 FM signals to be scaled to the initial I-atom absorption in order to compare results among different experiments. However, because the HO_2 line strength is not known, the yield of the HO_2 radical cannot be directly derived from the present data as it was in previous Cl-initiated alkyl + O_2 reactions.

The detection sensitivity of the infrared absorption technique is enhanced by employing a modified Herriott-type multipass flow cell.[34] The tunable infrared power is passed multiple times (17 or 21 passes) through the multipass flow cell. The flow cell is about 1.3 m long with CaF_2 windows and is surrounded by a commercial ceramic-fiber heater capable of reaching temperatures in excess of 1200 K. This arrangement allows the infrared probe to overlap the UV photolysis beam only in the center of the flow cell, where the temperature is more readily controlled. The effective path length (i.e., overlapping path of photolysis and probe beams) is between 9 and 11 m, depending on the number of passes through the flow cell.

An external-cavity tunable diode laser is employed to probe the time-resolved absorption profile of HO_2. To further improve the signal-to-noise ratio, the probe beam is split into signal and reference beams. The reference beam impinges on a low-noise detector (I_0), after traveling an equal path length as the signal beam, through an analogous modified Herriott-type multipass arrangement open to atmospheric pressure. The signal beam is directed through the multipass flow cell and onto a second low-noise detector (I). The time-resolved FM signal is monitored as the demodulated difference between balanced signal (I) and reference (I_0), permitting the subtraction of common noise. Approximately 50 μW of infrared power is incident on each detector. A commercial traveling-interferometer wavemeter is used to monitor the frequency of the diode laser beam.

The I-atom concentration is probed by a second external-cavity diode laser tuned to the $^2P_{1/2} \leftarrow {}^2P_{3/2}$ transition at ~1315 nm. The transient I-atom absorption is monitored by subtracting the output of balanced signal (I) and reference (I_0) detectors. To stabilize the frequency output of the diode laser, a fraction of the laser beam is phase-modulated, directed through a high-temperature cell (~1100 K), in which I_2 is thermally dissociated to generate I atoms, and imaged on a fast infrared detector. The resulting single-tone FM signal (after subsequent demodulation) is used as the "error signal" for a proportional−integral−derivative controller to automatically correct any frequency deviations away from line center.

Gas flows are controlled by calibrated mass flowmeters, and the total pressure is maintained by a butterfly valve at the exit of the cell, which operates under feedback from a capacitance manometer. The quartz flow cell is heated by three resistive elements, each under microprocessor control, with feedback from a separate K-type thermocouple.

Typical gas concentrations in the alkyl + O_2 study are [O_2] = 1.5×10^{17} cm^{-3} and [alkyl iodide] = $(1-2) \times 10^{15}$ cm^{-3}. Approximately 3% of the alkyl iodide molecules are photolyzed in the beam path volume. Helium is added to a total density of 3.65×10^{17} cm^{-3} (8.45×10^{17} cm^{-3} in some ethyl experiments). Experiments are carried out at four different temperatures (623, 648, 673, and 703 K). At the relatively high levels of O_2 in these experiments, I* atoms are quenched to the ground state very rapidly (on the order of a few microseconds)[35−38] and, thus, I-atom concentrations can be easily derived from the probe−laser path length (defined as the interaction path length between the photolysis laser and the 1315 nm probe) and the absolute absorption cross section of I atoms for the F* = 3 ← F = 4 hyperfine transition at 1315.246 nm.[39,40] I* relative quantum-yield determination studies are performed at 673 K and a total density of 3.65×10^{17} cm^{-3}. Oxygen concentrations in the I* branching-fraction measurements range from 5.0×10^{14} to 6.0×10^{15} cm^{-3}, and initial alkyl iodide concentrations are again kept in the range of $(1-2) \times 10^{15}$ cm^{-3}.

Theory of Alkyl + O_2 Reactions. The master-equation simulations have been performed as described in previous work on ethyl + O_2 and propyl + O_2, using the stationary-point energies calculated in previous works.[3,5,20,31] The ethyl + O_2 potential-energy surface has been described in detail elsewhere,[3,5,20] and no further details are presented here. The *n*-propyl + O_2 and *i*-propyl + O_2 potential-energy surfaces have also been described extensively in previous publications.[20,31] However, because one focus of the present work is to refine the model of the propyl + O_2 reactions, key earlier results are summarized below.

The primary pathway to HO_2 formation in the *n*-propyl and *i*-propyl + O_2 reactions is concerted elimination of HO_2 from $C_3H_7O_2$.[31,41,42] The elimination transition state is calculated to lie 5.2 kcal mol^{-1} below the energy of the reactants for *n*-C_3H_7 and 7.0 kcal mol^{-1} below the energy of the reactants for

TABLE 1: Rate Coefficients for the *i*-$C_3H_7 + O_2$ System Generated from Solutions to the Master Equation at a Total Density of 3.65×10^{17} cm^{-3}

reaction	k_{623}[a]	k_{648}[a]	k_{673}[a]	k_{703}[a]
i-$C_3H_7 + O_2 \rightarrow$ *i*-$C_3H_7O_2$	3.25×10^{-12}	2.65×10^{-12}	2.14×10^{-12}	1.63×10^{-12}
i-$C_3H_7 + O_2 \rightarrow$ *i*-C_3H_6OOH	5.96×10^{-16}	5.11×10^{-16}	4.39×10^{-16}	3.67×10^{-16}
i-$C_3H_7 + O_2 \rightarrow C_3H_6 + HO_2$	5.51×10^{-13}	5.41×10^{-13}	5.30×10^{-13}	5.16×10^{-13}
i-$C_3H_7 + O_2 \rightarrow$ methyloxirane + OH	1.87×10^{-14}	1.85×10^{-14}	1.83×10^{-14}	1.79×10^{-14}
i-$C_3H_7 + O_2 \rightarrow$ acetone + OH	8.15×10^{-16}	9.22×10^{-16}	1.04×10^{-15}	1.19×10^{-15}
i-$C_3H_7O_2 \rightarrow$ *i*-$C_3H_7 + O_2$	272	665	1.48×10^{3}	3.46×10^{3}
i-$C_3H_7O_2 \rightarrow$ *i*-C_3H_6OOH	0.607	1.40	3.09	7.55
i-$C_3H_7O_2 \rightarrow C_3H_6 + HO_2$	31.4	71.2	149	326
i-$C_3H_7O_2 \rightarrow$ methyloxirane + OH	0.601	1.30	2.52	4.65
i-$C_3H_7O_2 \rightarrow$ acetone + OH	3.01×10^{-3}	6.73×10^{-3}	1.37×10^{-2}	2.74×10^{-2}
i-$C_3H_6OOH \rightarrow$ *i*-$C_3H_7 + O_2$	1.50×10^{3}	2.38×10^{3}	3.66×10^{3}	5.90×10^{3}
i-$C_3H_6OOH \rightarrow$ *i*-$C_3H_7O_2$	1.29×10^{4}	1.61×10^{4}	1.95×10^{4}	2.37×10^{4}
i-$C_3H_6OOH \rightarrow C_3H_6 + HO_2$	5.50×10^{4}	7.85×10^{4}	1.09×10^{5}	1.52×10^{5}
i-$C_3H_6OOH \rightarrow$ methyloxirane + OH	9.93×10^{5}	1.33×10^{6}	1.74×10^{6}	2.31×10^{6}
i-$C_3H_6OOH \rightarrow$ acetone + OH	2.45×10^{-2}	3.89×10^{-2}	5.98×10^{-2}	9.56×10^{-2}

[a] Units of cm^3 molecule^{-1} s^{-1} for second-order reactions and s^{-1} for first-order reactions.

i-C_3H_7.[31] The 1,4 hydrogen shift to form QOOH is calculated at -2.6 kcal mol^{-1} for *n*-$C_3H_7 + O_2$ and -1.4 kcal mol^{-1} for *i*-$C_3H_7 + O_2$, again relative to the energies of the reactants. The transition state for the formation of OH from CH_3CHCH_2-OOH is 6.5 kcal mol^{-1} below the energy of *n*-$C_3H_7 + O_2$, and the transition state for HO_2 formation is 3.4 kcal mol^{-1} below the energy of the reactants. From *i*-C_3H_6OOH, the transition states for OH and HO_2 formation lie 4.9 and 1.9 kcal mol^{-1}, respectively, below the energy of the reactants. The *n*-$C_3H_7O_2$ radical has another possible isomerization, the 1,5 hydrogen shift to form $CH_2CH_2CH_2OOH$. This isomerization has a much lower barrier, 11.2 kcal mol^{-1} below the energy of the reactants, but $CH_2CH_2CH_2OOH$ has a sizable barrier to the formation of either OH or HO_2.[31] The barriers to formation of CH_3CHCH_2 via direct abstraction are 16.1 kcal mol^{-1} for *n*-propyl + O_2 and 13.0 kcal mol^{-1} for *i*-propyl + O_2.

For *n*-propyl + O_2, the barrier heights, and indeed the full model, are precisely as described in an earlier work,[31] including the minor adjustment of the energies made in order to reproduce the available experimental data.[20] In these revisions, the transition state for the elimination of HO_2 from $CH_3CH_2CH_2$-OO is raised by 1.4 kcal mol^{-1} from the ab initio value and the transition state for isomerization from $CH_3CH_2CH_2OO$ to CH_3-$CHCH_2OOH$ is also raised by 0.5 kcal mol^{-1}. For *i*-propyl + O_2, minor adjustments of the calculated potential energies also allow the time-resolved master-equation calculations to fit the available experimental data, including the present experimental data (as is described in the Results and Discussion section). These adjustments differ somewhat from those given in an earlier work[20] for a variety of reasons. In a previous computation of the rate coefficients for the *i*-propyl + O_2 reaction,[20] incorrect rotational constants were inadvertently used for some of the master-equation calculations. As a result, the adjustments to the stationary-point energies used to produce agreement with the available body of experimental work were somewhat in error, and they are corrected here. The $(CH_3)_2CHOO$ well depth is increased from the ab initio value by 1.3 kcal mol^{-1} and is now set at 38.1 kcal mol^{-1} below the energy of the reactants, and the transition state for HO_2 elimination is raised by 2 kcal mol^{-1} from the ab initio value of -7 kcal mol^{-1} to 5 kcal mol^{-1} below the energy of the reactants. In addition, the transition state for isomerization from $(CH_3)_2CHOO$ to $CH_3CH(CH_2)OOH$ is raised by 2.3 kcal mol^{-1}, as described previously.[20] Except for these changes, all of the barrier heights and other stationary points for both *n*-propyl + O_2 and *i*-propyl + O_2 are left as calculated from ab initio simulations.

For channels with a well-defined saddlepoint, the microcanonical rate coefficients have been evaluated on the basis of conventional transition-state theory. For the barrierless entrance channel, variable reaction-coordinate transition-state theory is employed. For propyl + O_2, the requisite transitional-mode potential is based on ab initio quantum evaluations at the B3LYP/6-31G* level of the energies along the minimum energy path.[31] An exponential down model is employed for the energy-transfer process. For ethyl + O_2, a temperature-independent value of $\Delta E_{down} = 200$ cm^{-1} is employed, as in prior work.[3,5,20] For propyl + O_2, a value of 350 cm^{-1} is instead employed, again independent of temperature.[20,31] The one-dimensional time-dependent master equation is solved via diagonalization of the transition matrix. The time-dependent populations of reactants, and unimolecular and bimolecular products, are determined directly from the eigenvalues and eigenvectors. The VARIFLEX[43] software is used in the master-equation simulations.

The results of the time-dependent master-equation analysis of ethyl + O_2 and propyl + O_2 reactions have been reduced to a set of elementary reactions and phenomenological rate coefficients that include pathways for HO_2 and OH formation. Phenomenological rate coefficients are obtained from solutions to the master equations using the methodology described by Klippenstein and Miller.[44] Table 1 shows the set of elementary reactions and phenomenological rate coefficients that are used to model the reaction of *i*-propyl + O_2 at 623, 648, 673, and 703 K, and a total density of 3.65×10^{17} cm^{-3}, using the modified stationary-point energies described above. Rate coefficients and equilibrium constants for ethyl + O_2 and *n*-propyl + O_2 are available from previous works,[5,20] as no further changes are performed here.

Comprehensive Kinetic Model. The calculated phenomenological rate coefficients for ethyl + O_2, *n*-propyl + O_2, and *i*-propyl + O_2 derived from the time-dependent master equations allow a model of the reaction systems to be constructed by using the elementary reactions involved in the three reaction systems. The experimentally observed HO_2 time traces can then be compared to predictions of this model. For these calculated phenomenological rate coefficients to reproduce the observed experimental data, rate coefficients must be added to the model that describe the loss and formation of all other radicals involved in the experiment, as performed previously.[20] Literature rate coefficients associated with these reactions are combined with the rate coefficients derived from the solutions to the master equations to form an integrated rate equation model that describes HO_2 formation and removal mechanisms important

TABLE 2: Reactions and Rate Coefficients Used To Model the HO_2 and I Signals from the Cl-Initiated Oxidation of Ethane and the Photodissociation of Ethyl Iodide[a]

reaction	A[b]	n	E_a/R (K)	reference
$C_2H_5 + O_2$ system				ME[c]
$C_2H_6 + Cl \rightarrow HCl + C_2H_5$	3.4×10^{-11}	0.7	−150	69
$HO_2 + HO_2 \rightarrow O_2 + H_2O_2$	2.2×10^{-13}		−600	64
$C_2H_5O_2 + C_2H_5O_2 \rightarrow 2C_2H_5O + O_2$	$\phi \times 8.5 \times 10^{-14}$		125	70[d]
$C_2H_5O_2 + C_2H_5O_2 \rightarrow C_2H_5OH + CH_3CHO + O_2$	$(1 - \phi) \times 8.5 \times 10^{-14}$		125	70[d]
$C_2H_5O_2 + HO_2 \rightarrow C_2H_5O_2H + O_2$	6.9×10^{-13}		−702	71
$C_2H_5 + C_2H_5 \rightarrow$ products	1.99×10^{-11}			72
$C_2H_5 + C_2H_5O_2 \rightarrow 2C_2H_5O$	4.0×10^{-11}			73[e]
$C_2H_5 + HO_2 \rightarrow OH + C_2H_5O$	3.3×10^{-11}			73[e]
$C_2H_5 + HO_2 \rightarrow O_2 + C_2H_6$	6.0×10^{-12}			73[e]
$C_2H_5 + C_2H_5O \rightarrow (C_2H_5)_2O$	2.0×10^{-12}			74
$C_2H_5O + O_2 \rightarrow HO_2 + C_2H_4O$	2.4×10^{-14}		325	75
$C_2H_5O + HO_2 \rightarrow H_2O_2 + C_2H_4O$	5.0×10^{-13}			73[e]
$C_2H_5O + C_2H_5O_2 \rightarrow C_2H_5OOH + C_2H_4O$	5.0×10^{-13}			73[e]
$C_2H_5O + C_2H_5O \rightarrow C_2H_5OH + CH_3CHO$	6.0×10^{-11}			*f*
$C_2H_5O \rightarrow CH_3 + CH_2O$	7.9×10^{13}		11060	76
$C_2H_5O \rightarrow H + C_2H_4O$	6.3×10^{13}		12100	76
$C_2H_5O \rightarrow CH_3CHOH$	5.0×10^{13}		13580	76
$C_2H_5O \rightarrow CH_2CH_2OH$	7.9×10^{12}		14830	76
$CH_3 + O_2 + M \rightarrow CH_3O_2 + M$				*g*
$CH_3O_2 + CH_3O_2 \rightarrow 2CH_3O + O_2$	9.2×10^{-14}		−390	70
$CH_3O_2 + C_2H_5O_2 \rightarrow CH_3 + C_2H_5O + O_2$	1.4×10^{-13}			*h*
$CH_3O + O_2 \rightarrow CH_2O + HO_2$	7.2×10^{-14}		1080	77
$H + O_2 + M \rightarrow HO_2 + M$				*i*
$Cl + C_2H_5 \rightarrow HCl + C_2H_4$	7.57×10^{-10}		290	78
$Cl + C_2H_5O_2 \rightarrow ClO + C_2H_5O$	7.7×10^{-11}			79
$Cl + C_2H_5O_2 \rightarrow HCl + C_2H_4O$	7.3×10^{-11}			79
$Cl + HO_2 \rightarrow ClO + OH$	4.1×10^{-11}		450	64
$Cl + HO_2 \rightarrow HCl + O_2$	1.8×10^{-11}		−170	64
$Cl + C_2H_5O \rightarrow C_2H_4O + HCl$	1.9×10^{-11}			*e*
$Cl_2 + C_2H_5 \rightarrow C_2H_5Cl + Cl$	1.3×10^{-11}		−120	80
$Cl_2 + CH_3 \rightarrow Cl + CH_3Cl$	4.8×10^{-12}		240	80
$Cl_2 + H \rightarrow Cl + HCl$	8.0×10^{-11}		209	81
$I + I + M \rightarrow I_2 + M$	5.5×10^{-34}		−575	82
$I + HO_2 \rightarrow HI + O_2$	1.47×10^{-11}		1090	68
$I + C_2H_5I \rightarrow I_2 + C_2H_5I$	1.69×10^{-10}		8600	83
$I + C_2H_5 \rightarrow HI + C_2H_4$	1.16×10^{-11}			84
$I + C_2H_5O_2 \rightarrow HOI + CH_3CHO$	2.0×10^{-12}			see text
$I + X \rightarrow$ products	1.0×10^{-11}			see text
$I_2 + OH \rightarrow HOI + I$	2.1×10^{-10}			75
$I_2 + C_2H_5 \rightarrow I + C_2H_5I$	5.0×10^{-11}			85
$HI + OH \rightarrow H_2O + I$	1.6×10^{-11}			75
$HI + C_2H_5 \rightarrow I + C_2H_6$	4.57×10^{-12}		−384	86
$C_2H_5I \rightarrow C_2H_5 + I$	4.5×10^{13}		25201	87
$C_2H_5I \rightarrow HI + C_2H_4$	1.27×10^{14}		26602	87

[a] Rate coefficients are written in the form $A(T/298)^n e^{-E_a/RT}$ unless otherwise noted. [b] Units of s^{-1} for first-order reactions, cm^3 molecule^{-1} s^{-1} for second-order reactions, and cm^6 molecule^{-2} s^{-1} for third-order reactions. [c] Rate coefficients are generated from solutions to the master equation (ME).[5,20] [d] The branching fraction is fit to the function $\phi = 1.33 \exp(-209/T)$.[70] [e] Estimated on the basis of the CH_3/O_2 system.[73] [f] Calculated based on an average of three literature studies.[73,88,89] [g] Effective second-order rate coefficient is calculated from the expression given by DeMore et al.[90] where $k_0^{300} = 4.5 \times 10^{-31}$ cm^6 molecule^{-2} s^{-1}, $k_\infty^{300} = 1.8 \times 10^{-12}$ cm^3 molecule^{-1} s^{-1}, $n = 3.0$, $m = 1.7$, and $F_{cent} = 0.6$. [h] Calculated based on an average of the rate coefficients of reaction $C_2H_5O_2 + C_2H_5O_2$ and reaction $CH_3O_2 + CH_3O_2$, assuming no temperature dependence (as estimated by Kaiser[6]). [i] Effective second-order rate coefficient is calculated from the expression given by DeMore et al.[90] where $k_0^{300} = 5.7 \times 10^{-32}$ cm^6 molecule^{-2} s^{-1}, $k_\infty^{300} = 7.5 \times 10^{-11}$ cm^3 molecule^{-1} s^{-1}, $n = 1.6$, $m = 0$, and $F_{cent} = 0.6$.

in the time domain of the experiment. The reactions and rate coefficients used in the model are listed in Table 2 for ethyl + O_2 and in Table 3 for propyl + O_2. Chlorine and iodine reactions are included jointly in the two master kinetic models. The experiments are initiated by either the photolysis of Cl_2 or the photolysis of alkyl iodides, and the model is adapted by setting the initial Cl- or I-atom concentration accordingly.

Several reactions appear in the model that have not been experimentally studied. The rate coefficients for these reactions are estimated by using rate coefficients for similar reactions. Estimates of several of these rate coefficients are based on similar reactions in the more thoroughly studied CH_3/O_2 system. In other cases, rate coefficients that have not been determined experimentally for the C_3H_7/O_2 systems are assumed to be identical to the analogous rate constants in the C_2H_5/O_2 system.

One important reaction that has not been experimentally studied is the reaction of RO_2 radicals with I atoms. However, the reaction

$$CF_3O_2 + I \rightarrow IO + CF_3O \qquad (3)$$

has been experimentally studied at room temperature by Wayne and co-workers[45] and is found to have a rate coefficient of 3.7×10^{-11} cm^3 molecule^{-1} s^{-1}. Some Br + alkyl radical reactions have also been measured experimentally to have smaller rate coefficients. Specifically, the rate coefficient for the reaction of Br + CH_3O_2 has been measured to be 4.4×10^{-13} cm^3 molecule^{-1} s^{-1},[46] and the rate coefficient for the reaction of CCl_3O_2 + Br has been measured to be 5.99×10^{-12} cm^3 molecule^{-1} s^{-1}.[47] A rate coefficient of 2×10^{-12} cm^3

TABLE 3: Reactions and Rate Coefficients Used To Model the HO_2 and I Signals from the Cl-Initiated Oxidation of Propane and the Photodissociation of *n*-Propyl Iodide and *i*-Propyl Iodide[a]

reaction	A[b]	n	E_a/R (K)	reference
$i\text{-}C_3H_7 + O_2$ system				ME[c]
$n\text{-}C_3H_7 + O_2$ system				ME[c]
$C_3H_8 + Cl \rightarrow HCl + n\text{-}C_3H_7$	1.12×10^{-10}		212	55
$C_3H_8 + Cl \rightarrow HCl + i\text{-}C_3H_7$	8.13×10^{-11}		86	55
$C_3H_8 + OH \rightarrow n\text{-}C_3H_7 + H_2O$	$\phi \times 1.87 \times 10^{-12}$	1.72	145	91[d]
$C_3H_8 + OH \rightarrow i\text{-}C_3H_7 + H_2O$	$(1-\phi) \times 1.87 \times 10^{-12}$	1.72	145	91[d]
$HO_2 + HO_2 \rightarrow O_2 + H_2O_2$	2.2×10^{-13}		−600	64
$OH + HO_2 \rightarrow H_2O + O_2$	4.8×10^{-11}		−250	64
$OH + OH \rightarrow O + H_2O$	6.2×10^{-14}	2.6	−945	75
$OH + OH + M \rightarrow H_2O_2 + M$	6.89×10^{-31}	−0.80		64
$n\text{-}C_3H_7O_2 + n\text{-}C_3H_7O_2 \rightarrow 2\ n\text{-}C_3H_7O + O_2$	$\phi \times 3.0 \times 10^{-13}$			64[e]
$n\text{-}C_3H_7O_2 + n\text{-}C_3H_7O_2 \rightarrow n\text{-}C_3H_7OH + C_2H_5CHO + O_2$	$(1-\phi) \times 3.0 \times 10^{-13}$			64[e]
$i\text{-}C_3H_7O_2 + i\text{-}C_3H_7O_2 \rightarrow 2i\text{-}C_3H_7O + O_2$	$\phi \times 1.6 \times 10^{-12}$		2200	64[e]
$i\text{-}C_3H_7O_2 + i\text{-}C_3H_7O_2 \rightarrow i\text{-}C_3H_7OH + CH_3COCH_3 + O_2$	$(1-\phi) \times 1.6 \times 10^{-12}$		2200	64[e]
$n\text{-}C_3H_7O_2 + i\text{-}C_3H_7O_2 \rightarrow n\text{-}C_3H_7O + i\text{-}C_3H_7O + O_2$				e, f
$n\text{-}C_3H_7O_2 + i\text{-}C_3H_7O_2 \rightarrow$ products				e, f
$n\text{-}C_3H_7O_2 + HO_2 \rightarrow n\text{-}C_3H_7O_2H + O_2$	6.9×10^{-13}		−702	g
$i\text{-}C_3H_7O_2 + HO_2 \rightarrow i\text{-}C_3H_7O_2H + O_2$	6.9×10^{-13}		−702	g
$n\text{-}C_3H_7O_2 + OH \rightarrow HO_2 + n\text{-}C_3H_7O$	4.0×10^{-11}			h
$i\text{-}C_3H_7O_2 + OH \rightarrow HO_2 + i\text{-}C_3H_7O$	4.0×10^{-11}			h
$C_3H_6OOH + O_2 \rightarrow HOOC_3H_6O_2$	3.98×10^{-12}	−0.44		i
$HOOC_3H_6O_2 \rightarrow C_3H_6OOH + O_2$	7.11×10^{16}	−2.45	17665	i
$HOOC_3H_6O_2 \rightarrow OH + HOOC_3H_5O$	1.98×10^{10}	3.27	13954	i
$HOOC_3H_6O_2 \rightarrow OH + HOOC_3H_5O$	1.37×10^{11}	3.19	19588	i
$HOOC_3H_6O_2 \rightarrow OH + OOC_3H_6O$	3.0×10^{15}		21905	i
$HOOC_3H_6O_2 \rightarrow HO_2 + C_3H_6O_2$	4.17×10^{10}	3.51	14331	i
$n\text{-}C_3H_7 + OH \rightarrow C_3H_6 + H_2O$	4.0×10^{-11}			92
$i\text{-}C_3H_7 + OH \rightarrow C_3H_6 + H_2O$	4.0×10^{-11}			92
$n\text{-}C_3H_7 + n\text{-}C_3H_7 \rightarrow n\text{-}C_6H_{14}$	1.7×10^{-11}			92
$n\text{-}C_3H_7 + n\text{-}C_3H_7 \rightarrow C_3H_6 + C_3H_8$	2.8×10^{-12}			92
$i\text{-}C_3H_7 + i\text{-}C_3H_7 \rightarrow i\text{-}C_6H_{14}$	1.0×10^{-11}	−0.7		92
$i\text{-}C_3H_7 + i\text{-}C_3H_7 \rightarrow C_3H_6 + C_3H_8$	6.5×10^{-12}	−0.7		92
$i\text{-}C_3H_7 + n\text{-}C_3H_7 \rightarrow C_6H_{14}$	2.91×10^{-11}	−0.35		92
$i\text{-}C_3H_7 + n\text{-}C_3H_7 \rightarrow C_3H_6 + C_3H_8$	1.16×10^{-11}	−0.35		92
$i\text{-}C_3H_7 + i\text{-}C_3H_7O_2 \rightarrow 2i\text{-}C_3H_7O$	1.66×10^{-11}			93
$i\text{-}C_3H_7 + n\text{-}C_3H_7O_2 \rightarrow i\text{-}C_3H_7O + n\text{-}C_3H_7O$	1.66×10^{-11}			j
$n\text{-}C_3H_7 + n\text{-}C_3H_7O_2 \rightarrow 2n\text{-}C_3H_7O$	1.66×10^{-11}			j
$n\text{-}C_3H_7 + i\text{-}C_3H_7O_2 \rightarrow i\text{-}C_3H_7O + n\text{-}C_3H_7O$	1.66×10^{-11}			j
$n\text{-}C_3H_7 + HO_2 \rightarrow OH + n\text{-}C_3H_7O$	3.3×10^{-11}			k
$i\text{-}C_3H_7 + HO_2 \rightarrow OH + i\text{-}C_3H_7O$	3.3×10^{-11}			k
$n\text{-}C_3H_7 + HO_2 \rightarrow O_2 + C_3H_8$	6.0×10^{-12}			k
$i\text{-}C_3H_7 + HO_2 \rightarrow O_2 + C_3H_8$	6.0×10^{-12}			k
$n\text{-}C_3H_7 + n\text{-}C_3H_7O \rightarrow n\text{-}(C_3H_7)_2O$	2.0×10^{-12}			l
$i\text{-}C_3H_7 + i\text{-}C_3H_7O \rightarrow i\text{-}(C_3H_7)_2O$	2.0×10^{-12}			l
$n\text{-}C_3H_7 + i\text{-}C_3H_7O \rightarrow (C_3H_7)_2O$	2.0×10^{-12}			l
$i\text{-}C_3H_7 + n\text{-}C_3H_7O \rightarrow (C_3H_7)_2O$	2.0×10^{-12}			l
$n\text{-}C_3H_7O + OH \rightarrow C_3H_6O + H_2O$	3.0×10^{-11}			k
$i\text{-}C_3H_7O + OH \rightarrow C_3H_6O + H_2O$	3.0×10^{-11}			k
$i\text{-}C_3H_7O + O_2 \rightarrow HO_2 + C_3H_6O$	1.6×10^{-14}		264.6	94
$n\text{-}C_3H_7O + O_2 \rightarrow HO_2 + C_3H_6O$	2.5×10^{-14}		240.6	94
$n\text{-}C_3H_7O + HO_2 \rightarrow H_2O_2 + C_3H_6O$	5.0×10^{-13}			k
$i\text{-}C_3H_7O + HO_2 \rightarrow H_2O_2 + C_3H_6O$	5.0×10^{-13}			k
$n\text{-}C_3H_7O + n\text{-}C_3H_7O_2 \rightarrow n\text{-}C_3H_7OOH + C_3H_6O$	5.0×10^{-13}			k
$i\text{-}C_3H_7O + i\text{-}C_3H_7O_2 \rightarrow i\text{-}C_3H_7OOH + C_3H_6O$	5.0×10^{-13}			k
$n\text{-}C_3H_7O + i\text{-}C_3H_7O_2 \rightarrow i\text{-}C_3H_7OOH + C_3H_6O$	5.0×10^{-13}			k
$i\text{-}C_3H_7O + n\text{-}C_3H_7O_2 \rightarrow n\text{-}C_3H_7OOH + C_3H_6O$	5.0×10^{-13}			k
$n\text{-}C_3H_7O + n\text{-}C_3H_7O \rightarrow n\text{-}C_3H_7OH + C_3H_6O$	6.0×10^{-11}			m
$i\text{-}C_3H_7O + i\text{-}C_3H_7O \rightarrow i\text{-}C_3H_7OH + C_3H_6O$	6.0×10^{-11}			m
$n\text{-}C_3H_7O + i\text{-}C_3H_7O \rightarrow C_3H_7OH + C_3H_6O$	6.0×10^{-11}			m
$i\text{-}C_3H_7O \rightarrow H + CO(CH_3)_2$	2.0×10^{14}		10800	95
$i\text{-}C_3H_7O \rightarrow CH_3 + CH_3CHO$	3.98×10^{14}		8660	95
$n\text{-}C_3H_7O \rightarrow C_2H_5 + CH_2O$	5.01×10^{13}		7850	96
$CH_3 + O_2 + M \rightarrow CH_3O_2 + M$				n
$CH_3O_2 + CH_3O_2 \rightarrow 2CH_3O + O_2$	9.2×10^{-14}		−390	70
$CH_3O + O_2 \rightarrow CH_2O + HO_2$	7.2×10^{-14}		1080	77
$C_2H_5 + C_2H_5 \rightarrow$ products	1.99×10^{-11}			72
$C_2H_5 + HO_2 \rightarrow OH + C_2H_5O$	3.3×10^{-11}			73[k]
$C_2H_5 + HO_2 \rightarrow O_2 + C_2H_6$	6.0×10^{-12}			73[k]

TABLE 3: Continued

reaction	A^b	n	E_a/R (K)	reference
$C_2H_5 + C_2H_5O \rightarrow (C_2H_5)_2O$	2.0×10^{-12}			74
$H + O_2 + M \rightarrow HO_2 + M$				*o*
n-$C_3H_7 \rightarrow C_3H_6 + H$	3.98×10^{13}		17608	97
n-$C_3H_7 \rightarrow C_2H_4 + CH_3$	6.95×10^{12}	−0.1	15211	98
i-$C_3H_7 \rightarrow C_3H_6 + H$	2.19×10^{12}	1.83	17819	99
i-$C_3H_7 \rightarrow C_2H_4 + CH_3$	3.98×10^{10}		14816	100
$Cl + n$-$C_3H_7 \rightarrow HCl + C_3H_6$	7.57×10^{-10}		290	*p*
$Cl + i$-$C_3H_7 \rightarrow HCl + C_3H_6$	7.57×10^{-10}		290	*p*
$Cl + n$-$C_3H_7O_2 \rightarrow ClO + n$-$C_3H_7O$	7.7×10^{-11}			*q*
$Cl + n$-$C_3H_7O_2 \rightarrow HCl + C_3H_6O_2$	7.3×10^{-11}			*q*
$Cl + i$-$C_3H_7O_2 \rightarrow ClO + i$-$C_3H_7O$	7.7×10^{-11}			*q*
$Cl + i$-$C_3H_7O_2 \rightarrow HCl + C_3H_6O_2$	7.3×10^{-11}			*q*
$Cl + HO_2 \rightarrow ClO + OH$	4.1×10^{-11}		450	64
$Cl + HO_2 \rightarrow HCl + O_2$	1.8×10^{-11}		−170	64
$Cl + n$-$C_3H_7O \rightarrow C_3H_6O + HCl$	1.9×10^{-11}			101[k]
$Cl + i$-$C_3H_7O \rightarrow C_3H_6O + HCl$	1.9×10^{-11}			101[k]
$Cl_2 + i$-$C_3H_7 \rightarrow Cl + i$-$C_3H_7Cl$	2.51×10^{-11}		−240	80
$Cl_2 + n$-$C_3H_7 \rightarrow Cl + n$-$C_3H_7Cl$	2.51×10^{-11}		−240	*r*
$Cl_2 + CH_3 \rightarrow Cl + CH_3Cl$	4.8×10^{-12}		240	80
$Cl_2 + H \rightarrow Cl + HCl$	8.0×10^{-11}		209	81
$I + I + M \rightarrow I_2 + M$	5.5×10^{-34}		−575	82
$I + HO_2 \rightarrow HI + O_2$	1.47×10^{-11}		1090	68
$I + n$-$C_3H_7I \rightarrow I_2 + n$-$C_3H_7$	2.09×10^{-10}		9301	102
$I + i$-$C_3H_7I \rightarrow I_2 + i$-$C_3H_7$	2.09×10^{-10}		9301	*s*
$I + n$-$C_3H_7 \rightarrow HI + C_3H_6$	1.16×10^{-11}			*t*
$I + i$-$C_3H_7 \rightarrow HI + C_3H_6$	1.16×10^{-11}			*t*
$I + n$-$C_3H_7O_2 \rightarrow HOI + C_2H_5CHO$	2.0×10^{-12}			see text
$I + i$-$C_3H_7O_2 \rightarrow HOI + CH_3COCH_3$	2.0×10^{-12}			see text
$I + X \rightarrow$ products	1.0×10^{-11}			see text
$I_2 + OH \rightarrow HOI + I$	2.1×10^{-10}			75
$I_2 + n$-$C_3H_7 \rightarrow n$-$C_3H_7I + I$	5.0×10^{-11}			85
$I_2 + i$-$C_3H_7 \rightarrow i$-$C_3H_7I + I$	5.0×10^{-11}			*u*
$HI + OH \rightarrow H_2O + I$	1.6×10^{-11}			75
$HI + n$-$C_3H_7 \rightarrow I + C_3H_8$	3.95×10^{-12}		−613	*v*
$HI + i$-$C_3H_7 \rightarrow I + C_3H_8$	3.95×10^{-12}		−613	86
n-$C_3H_7I \rightarrow n$-$C_3H_7 + I$	1.0×10^{13}		25201	103
n-$C_3H_7I \rightarrow HI + C_3H_6$	1.0×10^{13}		25201	103
i-$C_3H_7I \rightarrow HI + C_3H_6$	4.68×10^{13}		22701	104

[a] Rate coefficients are written in the form $A(T/298)^n e^{-E_a/RT}$ unless otherwise noted. [b] Units of s^{-1} for first-order reactions, cm^3 $molecule^{-1}$ s^{-1} for second-order reactions, and cm^6 $molecule^{-2}$ s^{-1} for third-order reactions. [c] Rate coefficients generated from solutions to the master equation (ME). [d] The branching fraction determined by Droege and Tully[91] has been fit to the function $\phi = -0.293 + 0.00286T - 3.47 \times 10^{-6}T^2 + 1.51 \times 10^{-9}T^3$. [e] Branching ratio to form C_3H_7O estimated on the basis of the C_2H_5/O_2 system.[70] [f] Estimated on the basis of the mean of the i-$C_3H_7O_2$ and n-$C_3H_7O_2$ self-reaction rate coefficients. [g] Literature value of $C_2H_5O_2 + HO_2$ is used as an estimate of the rate coefficient.[71] [h] Estimated on the basis of $CF_3O_2 + OH$.[105] [i] Estimated on the basis of $C_2H_5OOH + O_2$.[26] [j] Estimated on the basis of i-$C_3H_7 + i$-$C_3H_7O_2$.[93] [k] Estimated on the basis of the CH_3/O_2 system.[73] [l] Estimated on the basis of $C_2H_5O + C_2H_5$.[74] [m] Calculated on the basis of an average of three literature studies.[73,88,89] [n] Effective second-order rate coefficient is calculated from the expression given by DeMore et al.[90] where $k_0^{300} = 4.5 \times 10^{-31}$ cm^6 $molecule^{-2}$ s^{-1}, $k_\infty^{300} = 1.8 \times 10^{-12}$ cm^3 $molecule^{-1}$ s^{-1}, $n = 3.0$, $m = 1.7$, and $F_{cent} = 0.6$. [o] Effective second-order rate coefficient is calculated from the expression given by DeMore et al.[90] where $k_0^{300} = 5.7 \times 10^{-32}$ cm^6 $molecule^{-2}$ s^{-1}, $k_\infty^{300} = 7.5 \times 10^{-11}$ cm^3 $molecule^{-1}$ s^{-1}, $n = 1.6$, $m = 0$, and $F_{cent} = 0.6$. [p] Estimated on the basis of $C_2H_5 + Cl$.[78] [q] Estimated on the basis of $C_2H_5O_2 + Cl$.[79] [r] Estimated on the basis of $Cl_2 + i$-C_3H_7.[80] [s] Estimated on the basis of $I + n$-C_3H_7I.[102] [t] Estimated on the basis of $I + C_2H_5$.[84] [u] Estimated on the basis of $I_2 + n$-C_3H_7.[85] [v] Estimated on the basis of $HI + i$-C_3H_7.[86]

$molecule^{-1}$ s^{-1} is used in the present kinetic model for all three $I + RO_2$ reactions independent of temperature.

It is further necessary to include an additional loss of I atoms, namely, $I + X$, in the kinetic models in order to suitably simulate the I-atom profiles resulting from the photolysis of ethyl, *n*-propyl, and *i*-propyl iodides. A rate coefficient of 1.0×10^{-11} cm^3 $molecule^{-1}$ s^{-1} is employed in the simulations. All of the experimental I-atom decays exhibit second-order behavior, and, thus, good agreement between the models and the experimental data is found by setting the initial X-species concentration between the values of 0.5 and 0.85 of the initial I-atom concentration, depending on the experiment.

Results and Discussion

I* Yields. The I-atom photofragment resulting from the photodissociation of alkyl iodides is produced in both the electronic ground state and the spin−orbit-excited state, I*. The I atoms are produced with statistically populated hyperfine levels.[48−50] If a suitable concentration of quencher is introduced, ensuring a complete transfer of the initial I* population to ground-state I but still permitting resolution of the quenching time scale, the yield of I* can be accurately derived using gain versus absorption spectroscopy on the spin−orbit transition.[48−50] The technique of laser gain versus absorption spectroscopy involves monitoring of the time-resolved gain or absorption immediately after dissociation (initial signal amplitude $\equiv S_i$, positive for gain and negative for absorption), and the total absorption after quenching of I* to I is completed (final signal amplitude $\equiv S_f$, always positive). The ratio of the initial and final amplitudes (extrapolated to $t = 0$, which is the time when the laser fires) is directly related to the relative yield of the two states. Because of the finite time for the translational relaxation

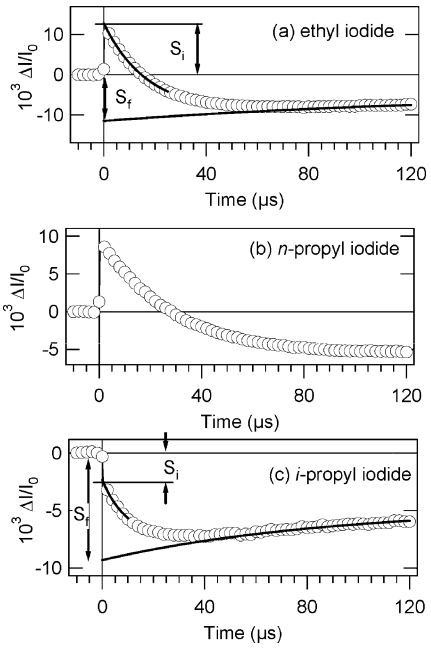

Figure 1. Transient absorption signals for (a) ethyl iodide, (b) *n*-propyl iodide, and (c) *i*-propyl iodide at 266 nm and 673 K. Only every 100th experimental point is shown for clarity. The technique of time-resolved laser gain vs absorption spectroscopy is employed in the determination of ϕ^*. This method involves the determination of the back-extrapolated time-zero amplitude (S_i), which is proportional to the degeneracy-weighted population difference of the I* and I atoms initially produced, and the long-time asymptotic amplitude (S_f), which is proportional to the total I-atom population generated by the photolysis pulse. These amplitudes are illustrated in parts a and c.

of I atoms, the initial amplitude is most reliably obtained from the extrapolation to $t = 0$ of an exponential fit to the quenching decay. Similarly, because of the reactive removal of I atoms at longer times, the final amplitude is derived from an exponential fit to the long-time decay.

Figure 1 displays typical I-atom transient absorption signals for ethyl, *n*-propyl, and *i*-propyl iodides obtained at 266 nm and at a temperature of 673 K. An illustration of the extrapolation used to derive amplitudes S_i and S_f is given by the solid lines. Only relative signal levels are required for the ϕ^* measurement. As developed by Leone and co-workers,[48−50] the relative I* quantum yield, ϕ^* {$\phi^* \equiv [I^*]/([I^*] + [I])$}, can be obtained from the following expression:

$$\phi^* = \frac{1}{3}\left(1 + \frac{S_i}{S_f}\right) \qquad (4)$$

where S_i, the initial back-extrapolated time-zero amplitude, is proportional to the population difference of the I and I* atoms initially produced (weighted by the state degeneracies) and S_f, the asymptotic long-time amplitude, is proportional to the total I-atom density generated by the photolysis pulse. Because of the state degeneracies, an initial gain is observed if the number of excited-state I* atoms exceeds half the number of ground-state I atoms ($\phi^* > {}^1/_3$); if $\phi^* < {}^1/_3$, initial absorption is seen. Very accurate quantum yields can be derived from laser gain versus absorption spectroscopy because of the independence of the measurement on parameters such as the concentrations of the precursor and the quenching gas, precise tuning of the probe laser, photolysis laser power, precursor absorption cross sections, and probe laser power.[48−50]

As seen in Figure 1, prompt gain is observed immediately after the photolysis pulse in the photodissociation of ethyl iodide and *n*-propyl iodide, indicating that the yield of I* is greater than ${}^1/_3$ for both molecules. In *i*-propyl iodide photolysis, a prompt absorption signal is visible, implying that the yield of I* is smaller than ${}^1/_3$. Subsequently, collisions with O_2 quench all of the I* atoms generated in the photodissociation, yielding ground-state I atoms (as observed by the increasing absorption signal). At longer times, ground-state atoms are removed from the probe volume by reaction with other species present in the photolysis mixture such as HO_2 and RO_2, leading to a decrease in the absorption signal.

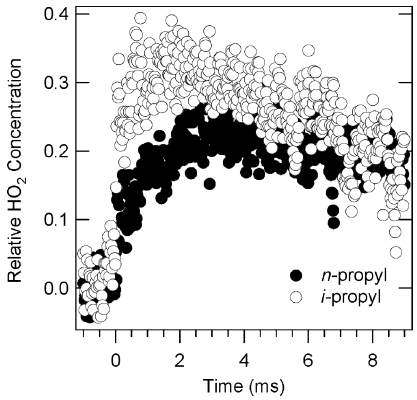

Figure 2. Experimental HO_2 time traces obtained by infrared FM spectroscopy taken in the photolysis experiments of *n*-propyl iodide (solid circles) and *i*-propyl iodide (open circles) at 648 K and a total density of 3.65×10^{17} cm^{-3}. Only every 20th point is shown for clarity.

The I* branching fractions, ϕ^*, are determined to be 0.68 ± 0.07 for ethyl iodide, 0.68 ± 0.07 for *n*-propyl iodide, and 0.25 ± 0.03 for *i*-propyl iodide. The spread among individual determinations is only a few percent; the uncertainty bounds include an estimate of possible systematic uncertainties such as errors in extrapolation. Uma and Das[51] have previously measured ϕ^* for ethyl iodide and *i*-propyl iodide at 266 nm using a two-photon laser-induced fluorescence scheme to probe the photofragments I and I*. They report yields of 0.72 ± 0.02 for ethyl iodide and 0.44 ± 0.03 for *i*-propyl iodide. The I* quantum yield for ethyl iodide reported from the present work is in good agreement with the yield determined by Uma and Das,[51] although they derive a higher I* yield for *i*-propyl iodide than what is obtained here. At least two measurements of ϕ^* for *i*-propyl iodide have been carried out at 248 nm, resulting in values between 0.23 and 0.26.[52,53] No measurements of ϕ^* have been reported at 266 nm for *n*-propyl iodide, although previously measured values for ϕ^* at 248 nm range from 0.56 to 0.60.[52,53]

Measurements and Modeling of HO_2 Production in Alkyl + O_2 Reactions. Figure 2 shows experimental HO_2 time traces obtained by infrared FM spectroscopy taken in the photolysis experiments of *n*-propyl iodide and *i*-propyl iodide at 648 K. The results depicted in this figure show clearly the differences between HO_2 formation in *i*-propyl and *n*-propyl oxidation and confirm that current experiments are sensitive probes of the reaction of both isomers with O_2. Similarly to other alkyl + O_2 reactions,[2,20,28−32] HO_2 formation is observed to occur on two different time scales: a prompt HO_2 signal, which is observed immediately following the UV flash and which cannot be temporally resolved under the current experimental conditions, and a second, slower delayed rise that becomes faster as the temperature is raised between 623 and 703 K (reflecting the reduced thermal stability of the alkylperoxy radical). The prompt HO_2 production is governed by the competition between

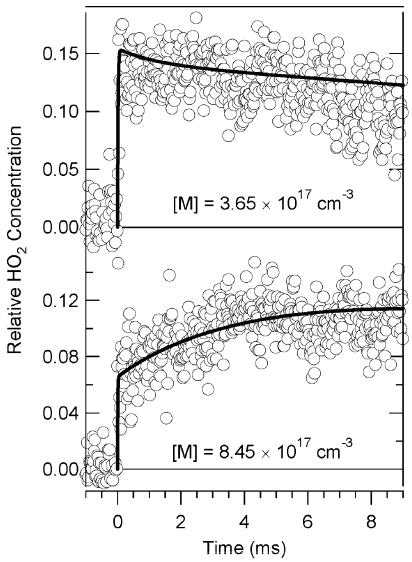

Figure 3. Comparison of the predicted (solid curve) and observed (circles) HO_2 produced in the photodissociation of ethyl iodide at 648 K and total densities of (a) 3.65×10^{17} cm^{-3} and (b) 8.45×10^{17} cm^{-3} obtained by infrared FM spectroscopy. Only every 20th point is shown for clarity.

collisional stabilization and direct reaction (concerted elimination of HO_2 from the chemically activated RO_2*). The longer-time-scale production of HO_2 arises from dissociation of the thermalized RO_2 species. HO_2 formation from the reaction of *i*-propyl + O_2 displays a bigger prompt yield and a faster secondary delayed production rate than those of the HO_2 formed from the *n*-propyl + O_2 reaction. Naturally, the next goal is to simulate both profiles with the integrated rate equation models.

A first test is to see whether the HO_2 production in the present ethyl iodide photolysis experiments is reproduced by the integrated rate equation model. The same parametrized master-equation rate coefficients that successfully modeled previous work[20] are used here, so this comparison tests the agreement of the present experiments with the Cl-initiated ethane oxidation studies. As can be observed in Figure 3, the kinetic model accurately reproduces the time behavior and amplitude of the HO_2 observed at the two different densities investigated.

The next step is to simulate the present isomeric propyl + O_2 experiments. Figures 4 and 5 show a comparison of the predicted and observed HO_2 and I signals at several temperatures in the *n*-propyl + O_2 experiments. The agreement between the experimental data and the model is very good for both HO_2 and I atoms for these experimental conditions. Figures 6 and 7 depict the same comparisons using similar experimental conditions, but this time for the *i*-propyl + O_2 experiments. The model underestimates the prompt HO_2 production, especially as the temperature increases, and displays slower secondary production rates than those observed experimentally. Even though the agreement between the experimental and modeled I-atom profiles in the *i*-propyl oxidation experiments is, in general, fairly good, the model does not capture the extra delayed rise in the I-atom concentration, which reduces the agreement between the model and the experimental data for approximately the first 4 ms after the flash.

To check consistency, the new integrated rate equation model has been employed to predict the HO_2 profiles obtained in previous Cl-initiated propane oxidation experiments.[28] The reaction of Cl atoms with propane forms both isomers of C_3H_7. For example, at 645 K, the Cl + propane reaction leads to the

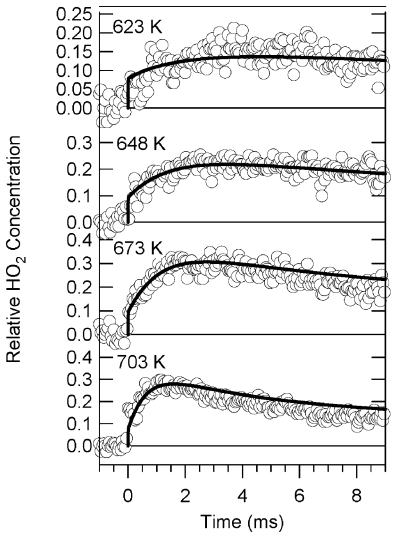

Figure 4. Comparison of the predicted (solid curve) and observed (circles) HO_2 produced in the photodissociation of *n*-propyl iodide at several temperatures and a total density of 3.65×10^{17} cm^{-3} obtained by infrared FM spectroscopy. Only every 50th point is shown for clarity.

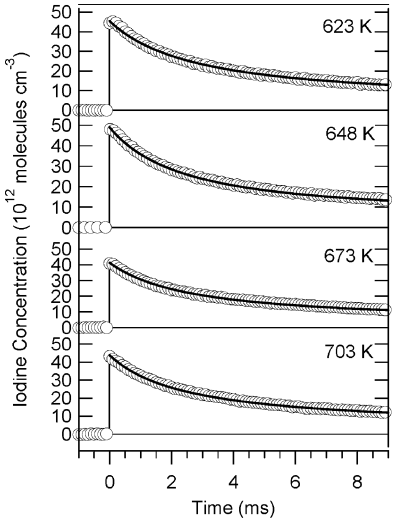

Figure 5. Comparison of the predicted (solid curve) and observed (circles) I-atom profiles produced in the photodissociation of *n*-propyl iodide at several temperatures and a total density of 3.65×10^{17} cm^{-3} obtained by infrared absorption spectroscopy. Observed I-atom concentrations are derived by using the absolute absorption cross section for the $F^* = 3 \leftarrow F = 4$ hyperfine transition of iodine atoms at 1.315 μm.[39,40] Only every 100th point is shown for clarity.

formation of the *n*-propyl radical ~53% of the time and to the *i*-propyl radical ~47% of the time.[54−56] Figure 8 shows a comparison between two experimental HO_2 traces obtained at a temperature of 645 K, and at two different total densities, and the present and previously employed kinetic models. The most significant difference between the two kinetic models is the somewhat different values for the rate coefficients for the elementary reaction steps involved in the *i*-propyl + O_2 reaction (as derived from solutions to master equations using the present stationary-point energies).[20] The present model reproduces the experimental traces very well and, in fact, does a better job of simulating the delayed HO_2 formation than the model used previously.[20]

Specific trends in the experimental and modeling results offer insight into the reaction mechanism. Figure 3 shows the HO_2 generated in the photodissociation of ethyl iodide at two different total densities but otherwise very similar experimental condi-

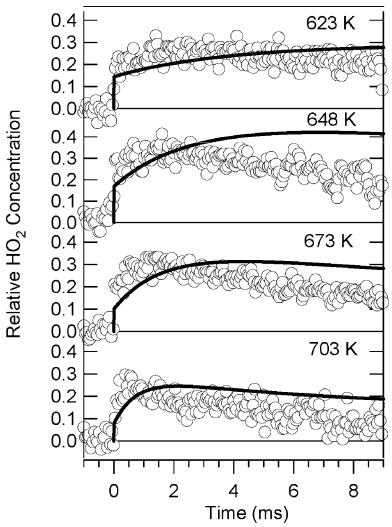

Figure 6. Comparison of the predicted (solid line) and observed (circles) HO_2 produced in the photodissociation of *i*-propyl iodide at several temperatures and a total density of 3.65×10^{17} cm^{-3} obtained by infrared FM spectroscopy. Only every 50th point is shown for clarity.

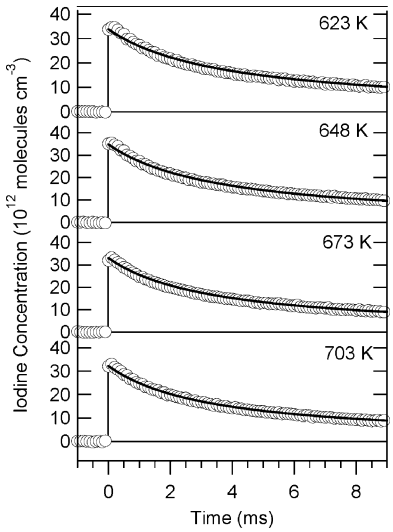

Figure 7. Comparison of the predicted (solid curve) and observed (circles) I-atom profiles produced in the photodissociation of *i*-propyl iodide at several temperatures and a total density of 3.65×10^{17} cm^{-3} obtained by infrared absorption spectroscopy. Observed I-atom concentrations are derived by using the absolute absorption cross section for the F* = 3 ← F = 4 hyperfine transition of iodine atoms at 1.315 μm.[39,40] Only every 100th point is shown for clarity.

tions. The relative prompt HO_2 production is a factor of 2 higher in the lower-density experiment, and only the higher-density experiment exhibits an evident secondary delayed production of HO_2. The decrease in prompt HO_2 with increasing pressure observed in Figure 3 reflects more efficient stabilization of the ethylperoxy radical, leading to a smaller initial yield of HO_2 molecules.[2,6,16,17]

The secondary HO_2 production reflects the escape of molecules from the R + O_2 ↔ RO_2 system via the concerted elimination transition state. This can be accomplished either by dissociation of RO_2 to R + O_2 followed by direct reaction or by thermal elimination of HO_2 from the stabilized RO_2 radical. For example, about 66% of the HO_2 yield in the lower-density measurement of Figure 3 is from this "delayed" production, whereas about 85% of the HO_2 in the higher-density experiment is formed by this mechanism. More efficient stabilization of the alkylperoxy radical at higher pressures naturally leads to more reactive flux through the stabilized RO_2 species. If the temperature is high enough that RO_2 dissociates on the time scale of the experiment, delayed HO_2 is observed from these stabilized RO_2 radicals.

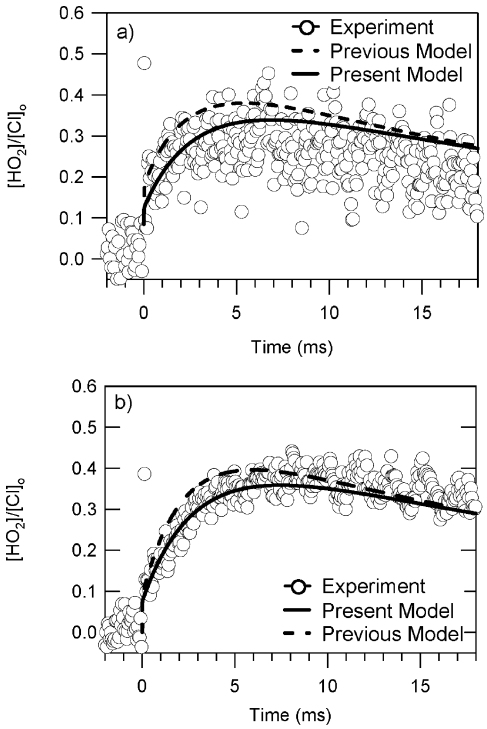

Figure 8. Comparison of the predicted (solid line) and observed (circles) HO_2 produced in the Cl-initiated oxidation of propane at 645 K and total densities of (a) 3.65×10^{17} cm^{-3} and (b) 8.45×10^{17} cm^{-3} obtained by infrared FM spectroscopy.[20,28] Also shown as a dashed curve for comparison is the predicted HO_2 generated by the previously employed kinetic model.[20] The experimental concentration is determined relative to the initial Cl-atom concentration using the reference Cl/CH_3OH/O_2 system. There is no arbitrary scaling of the amplitudes. Only every 10th experimental point is shown for clarity.

Figures 4 and 6 show how the time behavior of the HO_2 concentrations produced in the photodissociation of propyl iodides changes as a function of temperature at a constant density. Both the prompt and delayed productions of HO_2 increase as a function of temperature, as has been described previously.[28] As the temperature is raised, collisional stabilization of the propylperoxy radical becomes less effective as its thermal dissociation becomes faster. Concomitantly, the fraction of HO_2 molecules that are generated by direct reaction of R + O_2, whether in the initial reactive encounter or after dissociation of a propylperoxy radical, increases as the temperature is raised throughout the "transition regime" (∼580−750 K). As Miller and Klippenstein have thoroughly discussed,[5] as the transition regime is traversed from low to high temperatures (∼750 K), a "stabilization limit" is eventually reached, a temperature above which no collisional stabilization products can be formed, no matter how high the pressure. Therefore, in the high-temperature regime, HO_2 is formed purely by the direct reaction pathway and the prompt appearance of HO_2 is observed with no secondary production.

The prompt and delayed productions of HO_2 are both higher at each temperature in the *i*-propyl + O_2 reaction than they are in the *n*-propyl + O_2 reaction. Two major factors may contribute to the difference: the energy of the transition state for HO_2 elimination is lower with respect to the reactants in the *i*-propyl + O_2 reaction, and, entropically, the elimination transition state of the *i*-propylperoxy radical is favored because there are six

available H atoms in the two adjacent methyl groups in the *i*-propylperoxy radical versus two adjacent H atoms in the case of the *n*-propylperoxy radical. The overall effect is larger direct HO_2 production at each temperature in the *i*-propyl + O_2 reaction, which increases both prompt and delayed HO_2.

Before more fully discussing the possible impact of iodine chemistry and the photolysis of alkyl iodides on the experimental results, the results of the master-equation calculations are compared to other experiments in the literature. Theoretical results of the ethyl + O_2 reaction have been satisfactorily compared with measurements of total rate coefficients, HO_2 production rate coefficients, and HO_2 branching fractions,[3,5] and some of the experimental data have been used to successfully constrain key stationary-point energies on the ethyl + O_2 potential-energy surface. As an additional point of comparison, the ethyl kinetic model has been employed to reproduce the ethene percentage yields obtained by Kaiser[6] at three temperatures in his study of the mechanism of the ethyl + O_2 reaction. Kaiser's experiments involved the steady-state photolysis of mixtures containing Cl_2, C_2H_6, and O_2 over a wide temperature range (298−680 K) and a constant density of 6.8×10^{18} cm^{-3}. After a period of UV irradiation, the resulting mixtures are analyzed by gas chromatography/mass spectrometry to determine product yields. The present kinetic model predicts the following ethene yields under Kaiser's experimental conditions: 1.4% at 450 K, 31% at 550 K, and 87% at 650 K. These results are in good agreement with the experimental values obtained by Kaiser:[6] 1.3% at 450 K, 39% at 550 K, and 92% at 650 K.

The theoretical results of the *n*-propyl + O_2 reaction have been satisfactorily compared[31] to the measured total rate coefficients for *n*-propyl + O_2 from Slagle et al.[57] and Ruiz and Bayes.[58] In the present work, the propene yields obtained by Kaiser[59] are compared with the yields obtained by the propyl integrated rate equation model developed here using Kaiser's experimental conditions. Kaiser[59] investigated the generation of propene from the reaction of propyl + O_2 as a function of temperature (450−550 K) and at a constant density of 5.5×10^{18} cm^{-3} by irradiating mixtures of propane, Cl_2, and O_2. Because Kaiser[59] generates propyl radicals by the reaction of Cl with propane, both *n*-propyl and *i*-propyl radicals are formed in his experiments. The present propyl kinetic model results in the following propene yields under Kaiser's conditions: 0.5% at 450 K, 4% at 500 K, and 26% at 550 K. The calculated yields are in reasonable agreement with the values measured by Kaiser:[59] 0.7% at 450 K, 7% at 500 K, and 33% at 550 K.

Slagle and co-workers[9,60] have studied the equilibration of the reaction of *i*-propyl radicals + O_2 to form *i*-propylperoxy radicals over a range of temperatures (592−692 K) by monitoring the decay of *i*-propyl radicals with photoionization mass spectrometry. Figure 9 compares the results of the equilibrium constant derived by the master-equation calculations to the experimental values obtained by Slagle and co-workers.[9,60] The plot shows excellent agreement between the theory and the experiments. Gulati and Walker[61] have measured propene and propane yields, by gas chromatography, formed in the oxidation of isobutyraldehyde (over the temperature range of 653−773 K and a pressure of 50 Torr), and those results have been used to obtain rate coefficients for the reaction of *i*-propyl + O_2 to form propene. Master-equation calculations performed at 648, 703, 733, and 773 K and a total pressure of 50 Torr have been compared with the results obtained by Gulati and Walker,[61] and it is found that the simulated rate coefficients are within a factor of 2 of Gulati and Walker's values, within probable uncertainties

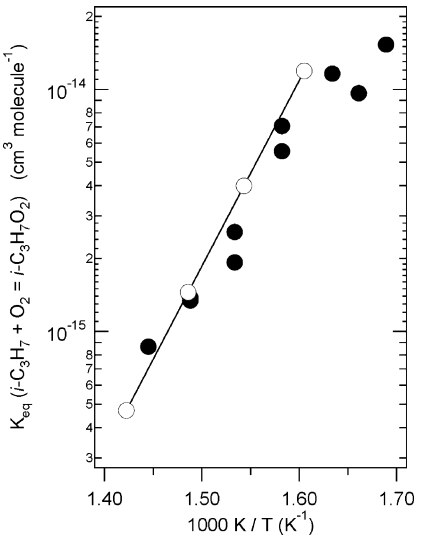

Figure 9. Comparison of the predicted (open circles) and measured (filled circles) equilibrium constants for the reaction of *i*-propyl + O_2 to form *i*-propylperoxy. The predicted equilibrium constants are derived from solutions to master equations, and the measured equilibrium constants are taken from the work of Knyazev and Slagle.[9]

of their determination. There is generally good agreement between the theoretical results reported here for ethyl, *n*-propyl, and *i*-propyl + O_2 reactions and the wide range of experimental results reported in the literature.

Iodine Chemistry. As depicted in Figure 7, the integrated rate equation model does not capture the delayed rise in the I-atom concentration observed in the *i*-propyl oxidation experiments (seen in the overshoot of the experiment at early time). Understanding this effect might provide clues as to the possible reasons for the systematic differences between the modeled and experimental HO_2 profiles in the *i*-propyl + O_2 experiments and to the identity of species X that has been introduced to model the I-atom decay. At least three possible explanations can be considered. The first possibility is that the I-atom absorption cross section might be changing over this initial time period as a result of velocity relaxation of I atoms as they collide with helium molecules (which leads to a change in Doppler shift). Cline et al.[62] have studied this effect by direct laser probing of I* Doppler profiles in the photodissociation of *n*-C_3F_7I at 266 nm. However, their experimental results indicate that velocity relaxation of I* atoms by He, which is expected to be very similar to relaxation of ground-state I atoms, occurs in approximately 50 collisions. This corresponds to a time of less than 1 μs, under the present experimental conditions, making this explanation unlikely. A second possibility involves the excited oxygen molecules produced in the quenching of I*:

$$I^* + O_2 \rightarrow I + O_2(^1\Delta) \qquad (5)$$

If the concentration of O_2 is not in large excess, then a significant equilibrium concentration of I* may be present at long times, leading to a competition between the re-emergence of I atoms and losses due to reactions with other species present in the oxidation system (which would manifest itself as a delayed rise in the I absorption profile). However, the equilibrium concentration of I* is negligible at the O_2 concentrations used in the present experiments. The third argument involves the effect of $O_2(^1\Delta)$ reactions on the overall chemistry. Because of the long radiative lifetime of $O_2(^1\Delta)$[63] and its slow quenching by bath gases,[64] including He, it is possible that $O_2(^1\Delta)$ may alter the chemistry of the experiments. However, a review of the

chemistry of $O_2(^1\Delta)$ reveals that $O_2(^1\Delta)$ reacts fairly slowly with most species of interest here, including alkenes.[65] Another piece of information that points away from $O_2(^1\Delta)$, or a product of it, as species X is that it appears necessary to set the initial concentration of species X to values higher than the measured yield of I* atoms resulting from the photodissociation of *i*-propyl iodide (i.e., $\phi^* = 0.25$).

Transient HO_2 FM signals are scaled on the basis of the initial I-atom absorption in order to compare results among different experiments because no internal calibration is available, as it was in previous Cl-initiated experiments. The key assumption in this comparison is that the initial I-atom concentration is equal to the initial alkyl-radical concentration. The simulated HO_2 profile is expressed as $[HO_2]_t/[R]_0$, but the experimental HO_2 signal is merely proportional to $[HO_2]_t$, with an unknown proportionality constant α that relates the HO_2 concentration to the FM signal amplitude. When the HO_2 signals are compared to those of the simulations, this detectivity constant (on the order of $\alpha = 10^{16}$ cm^{-3} V^{-1}) can be taken as an arbitrary scaling factor. However, although this constant is not precisely known, it should depend significantly, but predictably, only on temperature T and pressure p for identical probe-laser conditions. That is, the same concentration of HO_2 should give the same signal regardless of the photolysis source. The relative HO_2 signal does not depend on the initial alkyl iodide concentration, suggesting that pressure broadening by alkyl iodide is negligible under the present conditions. If $[R]_0$ is assumed to equal the measured initial I-atom concentration $[I]_0$, the experimental HO_2 yield $[HO_2]_t/[R]_0$ can be written in terms of the measured HO_2 signal FM(t) and the measured initial I-atom concentration:

$$\left[\frac{[HO_2]_t}{[R]_0}\right]_{exp} = \frac{\alpha(p,T)\ \mathrm{FM}(t)}{[R]_0} \approx \frac{\alpha(p,T)\ \mathrm{FM}(t)}{[I]_0} \qquad (6)$$

The proportionality constant α can be estimated by scaling the modeled $[HO_2]/[R]_0$ to the experimental ratio. However, matching the overall amplitudes of the model to the experimental HO_2 signals yields different values of the detectivity constant α for different alkyl radicals. Therefore, either α depends on the identity of the alkyl iodide in addition to its pressure and temperature dependence or the initial alkyl-radical concentration differs from the initial I-atom concentration. In the present simulations, the latter is assumed. Taking the minimum derived α to correspond to the case $[R]_0 = [I]_0$, the initial alkyl-radical concentration (compared to the initial I-atom concentration) is then reduced in the integrated rate equation model at the two highest temperatures investigated in the photolysis of *n*-propyl iodide and *i*-propyl iodide (depicted in Figures 4 and 6) and at all temperatures and pressures investigated in the photolysis of ethyl iodide (depicted in Figure 3). A reduction of the assumed initial alkyl-radical concentration, more pronounced at the highest temperature, is employed in the *n*-propyl and *i*-propyl oxidation models ($[R]_0/[I]_0$ factors ranging from 0.33 to 0.87), whereas a temperature-independent factor of $[R]_0/[I]_0 = 0.5$ is employed in the simulations of the ethyl oxidation system. Following the other possible assumption, a changing detectivity constant (or treating α as an arbitrary scaling constant) gives similar agreement between models and experimental traces. The reason for this scaling change is not completely clear.

It can be assumed that, for every I atom formed, one alkyl radical is initially formed. Nevertheless, it is conceivable that the excess energy of the photodissociation at 266 nm leads to the dissociation of some of the alkyl radicals before they are collisionally stabilized. A simple calculation using the experimental energy-partitioning results of Godwin et al.[52] and Kang et al.[66] and the ϕ^* measurements obtained from the present work indicates that the ethyl, *n*-propyl, and *i*-propyl radicals have, on average, approximately 12.5, 22, and 30.6 kcal mol^{-1} of internal energy, respectively, following the 266 nm photolysis pulse. Collisional deactivation of the alkyl radical is expected to take on the order of tens of microseconds,[67] which is adequate to thermalize the radicals before significant reaction with O_2 but perhaps not fast enough to prevent dissociation of the most highly excited alkyl radicals.

Although there is generally good agreement between the theoretical results reported in this work for the *i*-propyl + O_2 reaction and the wide range of experimental results reported in the literature, the present kinetic model does not completely accurately reproduce the experimental prompt HO_2 production and the secondary delayed HO_2 production, as described above. A number of possible sources exist for the discrepancy, including deficiencies in the experimental evidence and in the theoretical treatment. However, it must be recognized that the comparison of the master-equation calculations to the experimental results depends on the kinetics of a number of reactions beyond the R + O_2 system, including several reactions that have either never been studied or not been thoroughly studied. One such reaction is the reaction of I atoms with HO_2. This reaction has been experimentally studied over the temperature range of 283−353 K,[68] temperatures much lower than those employed in the present experimental studies. The Arrhenius expression provided by Jenkin et al.[68] has been used to extrapolate rate coefficients to the temperatures of this study. Another important reaction that has not been experimentally studied is the reaction of RO_2 radicals with I atoms, for which a rate coefficient of 2×10^{-12} cm^3 molecule^{-1} s^{-1} has been used to model all three I + RO_2 reactions independent of temperature. The integrated rate equation model predicts that these two reactions have a noticeable effect on both the observed HO_2 formation and the I-atom profile. The I + RO_2 reaction has a relatively bigger impact at the lower temperatures of the present experimental studies because RO_2 lives longer at these temperatures. The iodine decay cannot be even qualitatively modeled without a significant rate coefficient for the RO_2 + I reaction. Although it does not appear feasible to derive precise values for these rate coefficients from the present data, the combined experimental HO_2 and I profiles do constrain the values of certain critical rate coefficients, including I + RO_2 and I + HO_2.

Figure 10 shows a comparison of the predicted and observed HO_2 and I concentrations in the study of *i*-propyl + O_2 at 673 K. Both the experimental data and the simulated solid curves are the same as the ones shown in Figures 6 and 7, which employed the rate coefficients given in Table 3 for the simulations. The dashed curves employ the same model except that the rate coefficient for I + RO_2 has been increased by a factor of 10, to 2×10^{-11} cm^3 molecule^{-1} s^{-1} (a value closer to the room-temperature rate coefficient of 3.7×10^{-11} cm^3 molecule^{-1} s^{-1} determined by Wayne and co-workers in their study of the CF_3O_2 + I reaction[45]), and the rate coefficient for I + HO_2 has been increased by a factor of 3. Interestingly, the revised kinetic model accurately reproduces the experimental HO_2, but it does not, however, simulate the I trace as well as the previous model. A similar model can be employed to simulate the HO_2 and I experimental traces resulting from the photodissociation of *n*-propyl iodide. Figure 11 shows the comparison at 648 K, where, once again, the solid curves represent the same simulations as those displayed in Figures 4 and 5 and the dashed curves represent the revised model, where

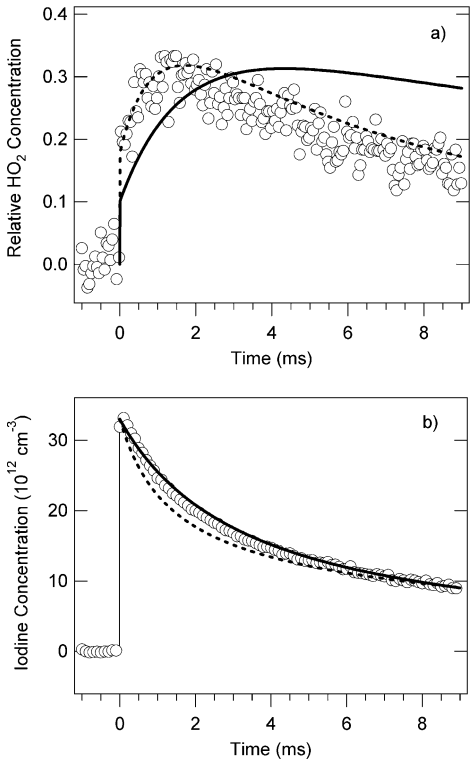

Figure 10. Comparison of the predicted (solid and dashed curves) and observed (circles) (a) HO_2 (every 50th point shown for clarity) and (b) I (every 100th point shown) produced in the photodissociation of *i*-propyl iodide at 673 K obtained by infrared FM spectroscopy. The solid curve is obtained by using the present kinetic model (as depicted in Figures 7 and 8), and the dashed curve is obtained by increasing the rate coefficients for I + RO_2 and I + HO_2 by factors of 10 and 3, respectively. Observed I-atom concentrations are derived by using the absolute absorption cross section for the F* = 3 ← F = 4 hyperfine transition of iodine atoms at 1.315 μm.[39,40]

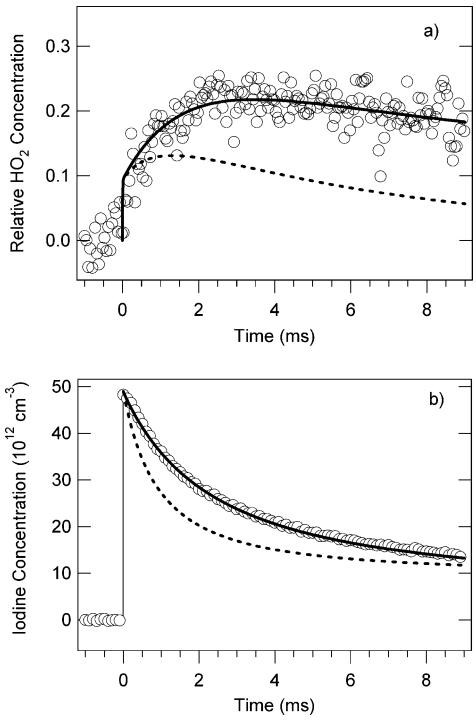

Figure 11. Comparison of the predicted (solid and dashed curves) and observed (circles) (a) HO_2 (every 50th point shown for clarity) and (b) I (every 100th point shown) produced in the photodissociation of *n*-propyl iodide at 648 K obtained by infrared FM spectroscopy. The solid curve is obtained by using the present kinetic model (as depicted in Figures 4 and 5), and the dashed curve is obtained by increasing the rate coefficients for I + RO_2 and I + HO_2 by factors of 10 and 3, respectively. Observed I-atom concentrations are derived by using the absolute absorption cross section for the F* = 3 ← F = 4 hyperfine transition of iodine atoms at 1.315 μm.[39,40]

it is now not necessary to include an additional loss of I atoms by reaction with species X. However, in this case, neither the HO_2 nor I experimental profile is modeled correctly, suggesting that the altered I + HO_2 and I + RO_2 rate coefficients employed in the revised simulations are not consistent with the wide range of experimental data obtained here. The change in the assumed HO_2 + I rate coefficient required to give significant improvement in modeling the experimental HO_2 production in the *i*-propyl + O_2 reaction cannot be reconciled with the ethyl + O_2 and *n*-propyl + O_2 data. Additionally, it is probably reasonable to assume that the reactions of I atoms with ethylperoxy, *n*-propylperoxy, and *i*-propylperoxy have similar rate coefficients, making a sizable increase in the assumed *i*-propyl−O_2 + I reaction unlikely. This comparison highlights the advantages of simultaneously probing two species, HO_2 and I, over a wide range of temperatures to demand consistency with theoretical simulations that partially depend on the kinetics of a number of reactions beyond the R + O_2 system but also points out the remaining uncertainties in the iodine chemistry.

Reliability of Adjusted Stationary-Point Energies. Other possible adjustments of theoretical parameters in the study of the *i*-propyl + O_2 reaction, such as the energies of stationary points along the calculated potential surface, energy-transfer constants, and collision cross sections, are less successful in accurately simulating the HO_2 profiles while maintaining consistency with the available literature data. For example, the elimination transition state of HO_2 from *i*-$C_3H_7O_2$ can be lowered by 1 kcal mol^{-1} and the *i*-$C_3H_7O_2$ well depth reduced by 1.3 kcal mol^{-1} (with respect to the adjusted stationary-point energies used to generate the phenomenological rate coefficients presented here). These changes lead to a higher prompt HO_2 production and a faster delayed HO_2 production, which fairly accurately reproduces the present experimental profiles (after the reduction of the *i*-propyl radical concentration with respect to the initial I concentration, as performed previously). However, the calculated rate coefficient for *i*-propyl + O_2 to form propene is then about a factor of 9 higher than the value derived in the experimental work of Gulati and Walker,[61] which is beyond the reasonable uncertainties for this value, and the agreement with experimental equilibrium constants[9] is diminished, inconsistencies that seem to invalidate this revision.

It is common in the study of complex reaction systems to derive experimental rate coefficients on the basis of an assumed kinetic mechanism. It may thus be tempting to simply extract rate coefficients for key elementary reactions in the alkyl + O_2 system using an optimization of the developed kinetic model. However, even if the set of elementary reactions that ultimately lead to HO_2 formation in the alkyl + O_2 system are reduced to four reactions (namely, reactions 1a, −1a, and 1b and the direct reaction of R + O_2 to form alkene + HO_2), additional experimental data (e.g., the RO_2 time profile) are necessary in order to have as many measured species as unknown rate coefficients in the system. Second, and more importantly, even if the assumed mechanism is complete and correct, the predicted rate coefficients depend on the kinetics of a number of reactions beyond the R + O_2 system, some of which have been discussed here. These facts lead to the present strategies of employing high-level computational kinetic methods for the prediction of rate coefficients in these systems and of restricting the optimiza-

tion of the resulting mechanism to minor adjustments of stationary-point energies within the estimated uncertainty of the quantum chemical method. The rate coefficients presented here reasonably reproduce the available kinetic data on alkyl + O_2 reactions while maintaining consistency with quantum chemical calculations.

Conclusions

New experimental measurements of HO_2 production resulting from the photolysis of ethyl iodide, *n*-propyl iodide, and *i* propyl iodide have been compared to integrated rate equation models based on the results of time-dependent master-equation calculations with ab initio characterization of stationary points. The production of HO_2 from the reaction of the two propyl isomers (*n*-propyl and *i*-propyl) with O_2 has been studied directly in the transition region. The current experiments unambiguously probe the reaction of each isomer with O_2 and permit isolation and refinement of the *i*-propyl + O_2 reaction model. The previous model accurately describes the time scale and amplitude of the HO_2 formation from both C_2H_5 + O_2 and *n*-C_3H_7 + O_2. However, the present revised model slightly underestimates the prompt HO_2 production and the slower, secondary production rate for *i*-propyl + O_2, although prediction of HO_2 formation in Cl-initiated propane oxidation has been improved. Measured I profiles have been employed to scale experimental HO_2 FM signals in order to compare results among different experiments and to place additional demands on the kinetic models. Although uncertainty remains concerning some of the iodine chemistry, the experimental results suggest significant rate coefficients for the I-atom reaction with alkylperoxy radicals.

Acknowledgment. The experiments reported here were facilitated by the outstanding technical support of Leonard E. Jusinski. This work is supported by the Division of Chemical Sciences, Geosciences, and Biosciences, Office of Basic Energy Sciences, U.S. Department of Energy. Sandia is a multiprogram laboratory operated by Sandia Corporation, a Lockheed Martin Company, for the National Nuclear Security Administration under Contract DE-AC04-94-AL85000.

References and Notes

(1) Ignatyev, I. S.; Xie, Y.; Allen, W. D.; Schaefer, H. F., III. *J. Chem. Phys.* **1997**, *107*, 141.
(2) Clifford, E. P.; Farrell, J. T.; DeSain, J. D.; Taatjes, C. A. *J. Phys. Chem. A* **2000**, *104*, 11549.
(3) Miller, J. A.; Klippenstein, S. J.; Robertson, S. H. *Proc. Combust. Inst.* **2000**, *28*, 1479.
(4) Rienstra-Kiracofe, J. C.; Allen, W. D.; Schaefer, H. F., III. *J. Phys. Chem A* **2000**, *104*, 9823.
(5) Miller, J. A.; Klippenstein, S. J. *Int. J. Chem. Kinet.* **2001**, *33*, 654.
(6) Kaiser, E. W. *J. Phys. Chem. A* **2002**, *106*, 1256.
(7) Pitz, W. J.; Westbrook, C. K. *Combust. Flame* **1986**, *63*, 113.
(8) Westbrook, C. K. *Proc. Combust. Inst.* **2000**, *28*, 1563.
(9) Knyazev, V. D.; Slagle, I. R. *J. Phys. Chem. A* **1998**, *102*, 1770.
(10) Slagle, I. R.; Ratajczak, E.; Gutman, D. *J. Phys. Chem.* **1986**, *90*, 402.
(11) Slagle, I. R.; Feng, Q.; Gutman, D. *J. Phys. Chem.* **1984**, *88*, 3648.
(12) Baldwin, R. R.; Pickering, I. A.; Walker, R. W. *J. Chem. Soc., Faraday Trans. 1* **1980**, *76*, 2374.
(13) McAdam, K. G.; Walker, R. W. *J. Chem. Soc., Faraday Trans. 2* **1987**, *83*, 1509.
(14) Walker, R. W.; Morley, C. Basic Chemistry of Combustion. In *Low-Temperature Combustion and Autoignition*; Pilling, M. J., Ed.; Elsevier: Amsterdam, 1997; p 1.
(15) Dobis, O.; Benson, S. W. *J. Am. Chem. Soc.* **1993**, *115*, 8798.
(16) Kaiser, E. W. *J. Phys. Chem.* **1995**, *99*, 707.
(17) Kaiser, E. W.; Lorkovic, I. M.; Wallington, T. J. *J. Phys. Chem.* **1990**, *94*, 3352.
(18) Kaiser, E. W.; Rimai, L.; Wallington, T. J. *J. Phys. Chem.* **1989**, *93*, 4094.
(19) Wagner, A. F.; Slagle, I. R.; Sarzynski, D.; Gutman, D. *J. Phys. Chem.* **1990**, *94*, 1853.
(20) DeSain, J. D.; Klippenstein, S. J.; Miller, J. A.; Taatjes, C. A. *J. Phys. Chem. A* **2003**, *107*, 4415.
(21) Stark, M. S. *J. Am. Chem. Soc.* **2000**, *122*, 4162.
(22) Quelch, G. E.; Gallo, M. M.; Schaefer, H. F., III. *J. Am. Chem. Soc.* **1992**, *114*, 8239.
(23) Quelch, G. E.; Gallo, M. M.; Shen, M.; Xie, Y.; Schaefer, H. F., III; Moncrief, D. *J. Am. Chem. Soc.* **1994**, *116*, 4953.
(24) Chen, C. J.; Bozzelli, J. W. *J. Phys. Chem. A* **2000**, *104*, 9715.
(25) Bozzelli, J. W.; Dean, A. M. *J. Phys. Chem.* **1990**, *94*, 3313.
(26) Bozzelli, J. W.; Sheng, C. *J. Phys. Chem. A* **2002**, *106*, 1113.
(27) Sheng, C. Y.; Bozzelli, J. W.; Dean, A. M.; Chang, A. Y. *J. Phys. Chem. A* **2002**, *106*, 7276.
(28) DeSain, J. D.; Clifford, E. P.; Taatjes, C. A. *J. Phys. Chem. A* **2001**, *105*, 3205.
(29) DeSain, J. D.; Klippenstein, S. J.; Taatjes, C. A. *Phys. Chem. Chem. Phys.* **2003**, *5*, 1584.
(30) DeSain, J. D.; Taatjes, C. A. *J. Phys. Chem. A* **2001**, *105*, 6646.
(31) DeSain, J. D.; Taatjes, C. A.; Miller, J. A.; Klippenstein, S. J.; Hahn, D. K. *Faraday Discuss.* **2001**, *119*, 101.
(32) DeSain, J. D.; Klippenstein, S. J.; Taatjes, C. A.; Hurley, M. D.; Wallington, T. J. *J. Phys. Chem. A* **2003**, *107*, 1992.
(33) Fink, E. H.; Ramsay, D. A. *J. Mol. Spectrosc.* **1997**, *185*, 304.
(34) Pilgrim, J. S.; Jennings, R. T.; Taatjes, C. A. *Rev. Sci. Instrum.* **1997**, *68*, 1875.
(35) Burde, D.; McFarlane, R. *J. Chem. Phys.* **1976**, *64*, 1850.
(36) Burrows, M. *J. Chem. Phys.* **1984**, *81*, 3546.
(37) Donovan, R. J.; Husain, D. *Chem. Rev.* **1970**, *70*, 489.
(38) Young, A.; Houston, P. *J. Chem. Phys.* **1983**, *78*, 2317.
(39) Ha, T.-K.; He, Y.; Pochert, J.; Quack, M.; Ranz, R.; Seyfang, G.; Thanopoulos, I. *Ber. Bunsen-Ges. Phys. Chem.* **1995**, *99*, 384.
(40) Davis, S.; Mulhall, P.; Bachman, M.; Kessler, W.; Keating, P. *J. Phys. Chem. A* **2002**, *106*, 8323.
(41) Chen, C.-J.; Bozzelli, J. W. *J. Phys. Chem. A* **2000**, *104*, 4997.
(42) Lay, T. H.; Bozzelli, J. W. *J. Phys. Chem. A* **1997**, *101*, 9505.
(43) Klippenstein, S. J.; Wagner, A. F.; Dunbar, R. C.; Wardlaw, D. M.; Robertson, S. H.; Miller, J. A. *VARIFLEX*, 1.12m ed.; Argonne National Laboratory: Argonne, IL, 2002.
(44) Klippenstein, S. J.; Miller, J. A. *J. Phys. Chem A* **2002**, *106*, 9267.
(45) Canosa-Mas, C. E.; Vipond, A.; Wayne, R. P. *Phys. Chem. Chem. Phys.* **1999**, *1*, 761.
(46) Aranda, A.; Laverdet, G.; Le Bras, G.; Poulet, G. *J. Chim. Phys. Phys.-Chim. Biol.* **1998**, *95*, 963.
(47) Fenter, F. F.; Lightfoot, P. D.; Niiranen, J. T.; Gutman, D. *J. Phys. Chem.* **1993**, *97*, 5313.
(48) Hess, W. P.; Kohler, S. J.; Haugen, H. K.; Leone, S. R. *J. Chem. Phys.* **1986**, *84*, 2143.
(49) Hess, W. P.; Leone, S. R. *J. Chem. Phys.* **1986**, *86*, 3773.
(50) Haugen, H. K.; Weitz, E.; Leone, S. R. *J. Chem. Phys.* **1985**, *83*, 3402.
(51) Uma, S.; Das, P. K. *J. Chem. Phys.* **1996**, *104*, 4470.
(52) Godwin, F. G.; Paterson, C.; Gorry, P. A. *Mol. Phys.* **1987**, *61*, 827.
(53) Brewer, P.; Das, P.; Ondrey, G.; Bersohn, R. *J. Chem. Phys.* **1983**, *79*, 720.
(54) Taatjes, C. A. Unpublished results. Measurements of rate coefficients and HCl yields from reactions of Cl with partially deuterated propanes suggest an *n*-propyl branching fraction of 0.53 ± 0.16 at 575 K.
(55) Tschuikow-Roux, E.; Niedzielski, J.; Faraji, F. *Can. J. Chem.* **1985**, *63*, 1093.
(56) Sarzynski, D.; Sztuba, B. *Int. J. Chem. Kinet.* **2002**, *34*, 651.
(57) Slagle, I. R.; Park, J.-Y.; Gutman, D. *Proc. Combust. Inst.* **1984**, *20*, 733.
(58) Ruiz, R. P.; Bayes, K. D. *J. Phys. Chem.* **1984**, *88*, 2592.
(59) Kaiser, E. W. *J. Phys. Chem. A* **1998**, *102*, 5903.
(60) Slagle, I. R.; Ratajczak, E.; Heaven, M. C.; Gutman, D.; Wagner, A. F. *J. Am. Chem. Soc.* **1985**, *107*, 1838.
(61) Gulati, S. K.; Walker, R. W. *J. Chem. Soc., Faraday Trans. 2* **1988**, *84*, 401.
(62) Cline, J. I.; Taatjes, C. A.; Leone, S. R. *J. Chem. Phys.* **1990**, *93*, 6543.
(63) Fisk, G. A.; Hays, G. N. *J. Chem. Phys.* **1982**, *77*, 4965.
(64) Atkinson, R.; Baulch, D. L.; Cox, R. A.; Hampson, R. F., Jr.; Kerr, J. A.; Rossi, M. J.; Troe, J. *J. Phys. Chem. Ref. Data* **1997**, *26*, 521.
(65) Ashford, R. D.; Ogryzlo, E. A. *J. Am. Chem. Soc.* **1975**, *97*, 3604.
(66) Kang, W. K.; Jung, K. W.; Kim, D. C.; Jung, K.-H.; Im, H.-S. *Chem. Phys.* **1995**, *196*, 363.
(67) Donaldson, D. J.; Leone, S. R. *J. Phys. Chem.* **1987**, *91*, 3128.
(68) Jenkin, M. E.; Cox, R. A.; Mellouki, A.; LeBras, G.; Poulet, G. *J. Phys. Chem.* **1990**, *94*, 2927.
(69) Pilgrim, J. S.; McIlroy, A.; Taatjes, C. A. *J. Phys. Chem. A* **1997**, *101*, 1873.

(70) Wallington, T. J.; Dagaut, P.; Kurylo, M. J. *Chem. Rev.* **1992**, *92*, 667.
(71) Maricq, M. M.; Szente, J. J. *J. Phys. Chem.* **1994**, *98*, 2078.
(72) Atkinson, D. B.; Hudgens, J. W. *J. Phys. Chem. A* **1997**, *101*, 3901.
(73) Tsang, W.; Hampson, R. F. *J. Phys. Chem. Ref. Data* **1986**, *15*, 1087.
(74) Foucaut, J.-F.; Martin, R. *J. Chim. Phys. Phys.-Chim. Biol.* **1978**, *75*, 132.
(75) Atkinson, R.; Baulch, D. L.; Cox, R. A.; Crowley, J. N.; Hampson, R. F., Jr.; Kerr, J. A.; Rossi, M. J.; Troe, J. *Summary of Evaluated Kinetic and Photochemical Data for Atmospheric Chemistry: IUPAC Subcommittee on Gas Kinetic Data Evaluation for Atmospheric Chemistry*. http://www.iupac-kinetic.ch.cam.ac.uk (Nov 2003).
(76) Hoyermann, K. O. M.; Seeba, J.; Viskolcz, B. *J. Phys. Chem. A* **1999**, *103*, 5692.
(77) Atkinson, R. *Int. J. Chem. Kinet.* **1997**, *29*, 99.
(78) Maricq, M. M.; Szente, J. J.; Kaiser, E. W. *J. Phys. Chem.* **1993**, *97*, 7970.
(79) Maricq, M. M.; Szente, J. J.; Kaiser, E. W.; Shi, J. *J. Phys. Chem.* **1994**, *98*, 2083.
(80) Timonen, R. *Ann. Acad. Sci. Fenn., Ser. A2* **1988**, *218*, 5.
(81) Berho, F.; Rayez, M.; Lesclaux, R. *J. Phys. Chem. A* **1999**, *103*, 5501.
(82) Baulch, D. L.; Duxbury, J.; Grant, S. J.; Montague, D. C. *J. Phys. Chem. Ref. Data* **1981**, *10* (Suppl. 1).
(83) Hartley, D. B.; Benson, S. W. *J. Phys. Chem.* **1963**, *39*, 132.
(84) Hunter, T. F.; Kristjansson, K. S. *J. Chem. Soc., Faraday Trans. 2* **1982**, *78*, 2067.
(85) Hayes, D. M.; Strong, R. L. *J. Phys. Chem.* **1986**, *90*, 6305.
(86) Seetula, J. A.; Russell, J. J.; Gutman, D. *J. Am. Chem. Soc.* **1990**, *112*, 1347
(87) Yang, J. H.; Conway, D. C. *J. Chem. Phys.* **1965**, *43*, 1296.
(88) Hassinen, E.; Koskikallio, J. *Acta Chem. Scand., Ser. A* **1979**, *33*, 625.
(89) Yee Quee, M. J.; Thynne, J. C. J. *Ber. Bunsen-Ges. Phys. Chem.* **1968**, *72*, 211.
(90) DeMore, W. B.; Sander, S. P.; Golden, D. M.; Hampson, R. F.; Kurylo, M. J.; Howard, C. J.; Ravishankara, A. R.; Kolb, C. E.; Molina, M. J. *Chemical Kinetics and Photochemical Data for Use in Stratospheric Modeling*; Jet Propulsion Laboratory: Pasadena, CA, 1997.
(91) Tully, F. P.; Droege, A. T.; Koszykowski, M. L.; Melius, C. F. *J. Phys. Chem.* **1986**, *90*, 691.
(92) Tsang, W. *J. Phys. Chem. Ref. Data* **1988**, *17*, 887.
(93) Munk, J.; Pagsberg, P.; Ratajczak, E.; Sillesen, A. *Chem. Phys. Lett.* **1986**, *132*, 417.
(94) Fittschen, C.; Frenzel, A.; Imrik, K.; Devolder, P. *Int. J. Chem. Kinet.* **1999**, *31*, 860.
(95) Batt, L. *Int. J. Chem. Kinet.* **1979**, *11*, 977.
(96) Choo, K. Y.; Benson, S. W. *Int. J. Chem. Kinet.* **1981**, *13*, 833.
(97) Kerr, J. A.; Trotman-Dickenson, A. F. *Trans. Faraday Soc.* **1959**, *55*, 572.
(98) Bencsura, Á.; Knyazev, V. D.; Xing, S.-B.; Slagle, I. R.; Gutman, D. *Proc. Combust. Inst.* **1992**, *24*, 629.
(99) Seakins, P. W.; Robertson, S. H.; Pilling, M. J.; Slagle, I. R.; Gmurczyk, G. W.; Bencsura, A.; Gutman, D.; Tsang, W. *J. Phys. Chem.* **1993**, *97*, 4450.
(100) Kerr, J. A.; Trotman-Dickenson, A. F. *Trans. Faraday Soc.* **1959**, *55*, 921.
(101) Daele, V.; Laverdet, G.; Poulet, G. *Int. J. Chem. Kinet.* **1996**, *28*, 589.
(102) Sullivan, J. H. *J. Phys. Chem.* **1961**, *65*, 722.
(103) Butler, E. T.; Polanyi, M. *Trans. Faraday Soc.* **1943**, *39*, 19.
(104) Tsang, W. *J. Phys. Chem.* **1964**, *41*, 2487.
(105) Biggs, P.; Canosa-Mas, C. E.; Shallcross, D. E.; Vipond, A.; Wayne, R. P. *J. Chem. Soc., Faraday Trans.* **1997**, *93*, 2701.